Candidate Denisovan fossils identified through gene regulatory phenotyping

Nadav Mishol[1,2,3], Gadi Herzlinger[4], Yoel Rak[5], Uzy Smilanksy[6], Liran Carmel[2], and David Gokhman[1]

[1]Department of Molecular Genetics, Weizmann Institute of Science, Rehovot, Israel.

[2]Department of Genetics, The Hebrew University of Jerusalem, Jerusalem, Israel.

[3]Institute of Archeology, The Hebrew University of Jerusalem, Israel.

[4]Zinman Institute of Archaeology, School of Archaeology and Maritime Cultures, University of Haifa, Israel.

[5]Sackler Faculty of Medicine, Tel-Aviv University, Israel.

[6]Department of Physics of Complex Systems, The Weizmann Institute of Science, Israel

April 2024

1 Abstract

Denisovans are an extinct group of humans whose morphology is mostly unknown. The scarcity of verified Denisovan fossils makes it challenging to study how they differed in their anatomy, and how well they were adapted to their environment. To gain insight into their evolutionary history, we used a genetic phenotyping approach, where Denisovan anatomy was inferred by detecting gene regulatory changes that likely altered Denisovan skeletal morphology. We then scanned

Middle Pleistocene skulls for unclassified specimens that match our Denisovan profile and thus might have been related to Denisovans. We found that the Harbin, Dali, and Kabwe specimens show a particularly good match to the predicted Denisovan profile. We conclude that our genetic phenotyping approach could help classify unidentified specimens, and that Harbin, Dali, and Kabwe likely belonged to individuals closely linked to the Denisovan lineage.

2 Introduction

Denisovans are an extinct human lineage that likely shared a common ancestor with Neanderthals 390-440 thousand years ago [1, 2, 3, 4]. The first Denisovan finding was reported in 2010 based on DNA extracted from the distal phalanx of a fifth finger [2]. Since then, nine additional specimens (as well as sediment DNA) have been attributed to Denisovans based on their DNA or protein sequences [1]. This collection includes three molars [5, 3], a long bone fragment [3], a partial parietal bone (unpublished), half a mandible with two molars [6] and three undiagnostic bone fragments [7]. These remains revealed several aspects of Denisovan morphology, including their large molars [2], a fifth distal phalanx resembling that of anatomically modern humans (AMHs) [8], and an archaic mandibular morphology which includes a robust and relatively low and thick body, without a developed chin [6]. However, the number of confirmed Denisovan specimens is still considerably lower than that of Neanderthals, hindering our ability to study Denisovan adaptations and phenotypic evolution.

The majority of confirmed Denisovan remains have been discovered within the Denisova Cave in Siberia. Nevertheless, a growing body of evidence indicates that their geographical presence extended further to the east and south. This evidence includes the Denisovan sediment DNA and mandible found in the Tibetan plateau [9, 6], a tooth from Laos assumed to be Denisovan [10], a mandible from Taiwan [11] exhibiting similarities in dental and mandibular morphology to Denisovans, and admixture with populations from East Asia, Southeast Asia, South Asia, and Oceania [1]. Thus, it is likely that Denisovans inhabited an extensive geographical range.

Meanwhile, many hominin specimens dated to the Middle and Upper Pleistocene remain poorly classified. The fossil record of these periods is poorly characterized, and the ability to genetically categorize these remains is limited. Consequently, certain specimens have been classified as new provisional lineages

(e.g., H. *cepranensis* [12, 13], H. *bodoensis* [14], and H. *daliensis*), while others have been grouped together into broad and highly variable taxonomic groups such as H. *heidelbergensis*. The difficulty in defining and classifying fossils from this period is often referred to as "The Muddle in the Middle" [15].

Importantly, many of these debated specimens have been found in East and Southeast Asia, i.e., in the likely habitat of Denisovans. Notable cranial examples include *Harbin* [16], *Dali* [17], *Jinniushan* [18], *Xuchang* [19], *Xujiayao* [20], *Hualongodng* [21] and *Penghu* [11]. Some researchers advocate for their classification as independent species [16, 22], while others have suggested they are eastern representatives of H.*heidelbergenis* [23], or local variants of archaic H. *sapiens* [24]. It has also been proposed that some of these specimens might actually be Denisovans [25, 1]. Nonetheless, the challenge to substantiate this claim lies in the scarcity of morphologically informative Denisovan remains on one hand, and the lack of genetic and proteomic data from these specimens on the other hand. In other words, to classify specimens that lack genetic data as Denisovans, who are defined through their genome, it is imperative to bridge the gap between genetics and morphology. This can be achieved by extracting phenotypic information from the Denisovan genome and comparing it against candidate specimens.

We have previously developed a method that utilizes gene regulatory data to compare two individuals and discern which one has the higher phenotypic value (e.g., taller stature) [26]. This method is based on two key conjectures: (i) substantial alterations to gene regulation are likely to have resulted in phenotypic changes, and (ii) the direction of phenotypic change following gene down-regulation is likely the same as the direction of phenotypic change in cases of gene loss-of-function [26]. To detect gene regulatory changes between the Denisovan, Neanderthal, and modern human lineages, we leveraged our previously published maps of a key regulatory mark of the genome - DNA methylation [27][28]. By linking observations of gene down-regulation with the reported

phenotypic consequences of gene loss-of-function, we constructed a genetically inferred morphological profile. We first tested this approach by reconstructing a profile of Neanderthal and chimpanzee anatomy and compared them against their known morphology. We found that this method has a prediction accuracy of over 85%. Then, we applied it to the Denisovan lineage, providing 32 skeletal traits that likely separated it from Neanderthals, modern humans, or both. These predictions were qualitative rather than quantitative in the sense that they provided the direction, but not the precise extent, of change. For instance, while it suggests that Denisovans likely exhibited a larger biparietal width compared to both Neanderthals and modern humans, the exact magnitude of this difference cannot be determined [26].

Morphologically informative Denisovan specimens published after the reconstruction of the profile, which include several molars, a mandible, and a phalanx, could potentially be used to further evaluate the accuracy of the Denisovan profile. However, only in a minority of cases these findings could be directly compared with the predicted profile. The Xiahe mandible [9] exhibits a high resemblance to the Denisovan profile, with seven out of eight correct predictions [26]. The Denisova 3 distal phalanx [8] could potentially be used to test the prediction of reduced tapering of the finger from base to fingertip in Denisovans compared to AMHs. However, this comparison requires a Denisovan proximal phalanx, which has not been found to date, leaving the accuracy of this prediction to be determined. Finally, despite the availability of Denisovan molars, our predictions of Denisovan dentition relate to the timing of tooth eruption and loss, which cannot be determined using current specimens (see Methods for *tooth enamel*).

Here, we use the reconstructed Denisovan profile to scan the Middle Pleistocene fossil record for crania whose morphology matches the profile and thus might have belonged to Denisovans or their close relatives.

3 Results

3.1 Test subjects and measurements

Most measurements used in this analysis were taken directly from the Morphobank dataset of Ni *et al* 2021 [16].

To scan the fossil record for specimens matching the reconstructed Denisovan profile, we started by defining a set of test specimens using several criteria. First, we only examined specimens whose dating partially or completely post-dates the emergence of the Denisovan lineage, i.e., the estimated Denisovan-Neanderthal split (390-440 kya, [4]). Second, crania that have been firmly classified as belonging to a non-Denisovan lineage (e.g., Neanderthals, *Homo erectus*, and AMHs) were excluded from the main analysis and were instead used as controls. Specimens classified as *Homo heidelbergensis* were included in the analysis because of the ongoing debate around their classification (e.g., [29, 30] and their phylogenetic proximity to Denisovans, suggesting that some of these specimens perhaps belong to Denisovans [25]. Third, for a single specimen to be informative, it must contain various traits that can be examined against the profile. As the Denisovan profile contains many predictions for the cranial region, we focused on sufficiently complete cranial specimens, containing at least five traits that can be tested against the profile. Given the possibility that the Denisovan habitat extended beyond the geographic range of Easter Eurasia, we did not filter out specimens based on their location. Altogether, the set of well-preserved Middle Pleistocene cranial fossils included nine well-preserved specimens (hereafter, *test subjects*, Fig. 1). These test subjects lack genetic characterization, display substantial morphological diversity, and their phylogenetic relationship to known hominin groups is uncertain or subject to debate.

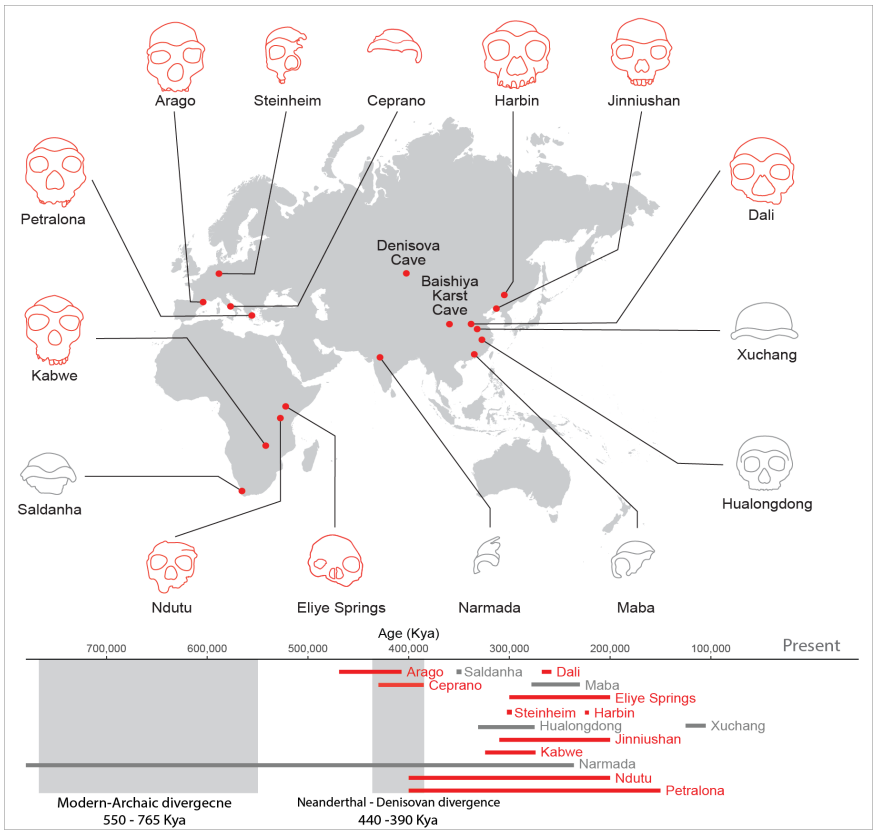

Figure 1: Test subjects examined for anatomical resemblance to predicted Denisovan anatomy. In red are adult test subjects with sufficient measurements for comparison. Sites with confirmed Denisovan findings are highlighted - Denisova Cave where Denisovans were first identified, and Baishiya Karst Cave where the Xiahe mandible was found. Below: estimated ranges of the test subject ranges. Crania are not shown to scale.

The reconstructed Denisovan cranial profile included directional predictions of 18 traits in which Denisovans are expected to differ from AMHs, Neanderthals, or both. 3 of these traits are non-morphometric (teeth loss timing, teeth eruption timing, enamel thickness), rendering them unquantifiable in the test subjects. Out of the remaining 15 traits, 10 can be measured based on the cranium alone (excluding the mandible). Since all test subjects don't have an available

mandible, only those 10 measurements were analyzed. The others were tested separately in a mandibular-specific analysis.

Out of the 10 measurements, 7 of the traits were taken from the Morphobank dataset [16] for the test subjects, as well as for the control groups.For the other 3 for which the Morphobank dataset had no available information (calvarial curvature, forehead height, and glabellar protrusion), were measured by us based on the supplementary images provided by the authors. Overall, our analyses investigated ten cranial traits (Fig. 2A-B).

In all ten traits, our predicted profile indicated that Denisovans differed from AMHs, and in four of them, Denisovans were also predicted to differ from Neanderthals (Fig. 2B). Thus, depending on the degree of specimen preservation, up to 14 comparisons were carried out for each test subject. In each comparison, the test subject was compared against the range of morphometric measurements in the hominin group from which Denisovans were predicted to differ. For instance, our profile suggested that Denisovans had a lower forehead compared to AMHs. We therefore compared forehead height in each test subject against the range of forehead heights observed in AMHs. If a test subject's forehead height fell below the median value of forehead heights in AMHs, it was considered a match (Fig. 2C).

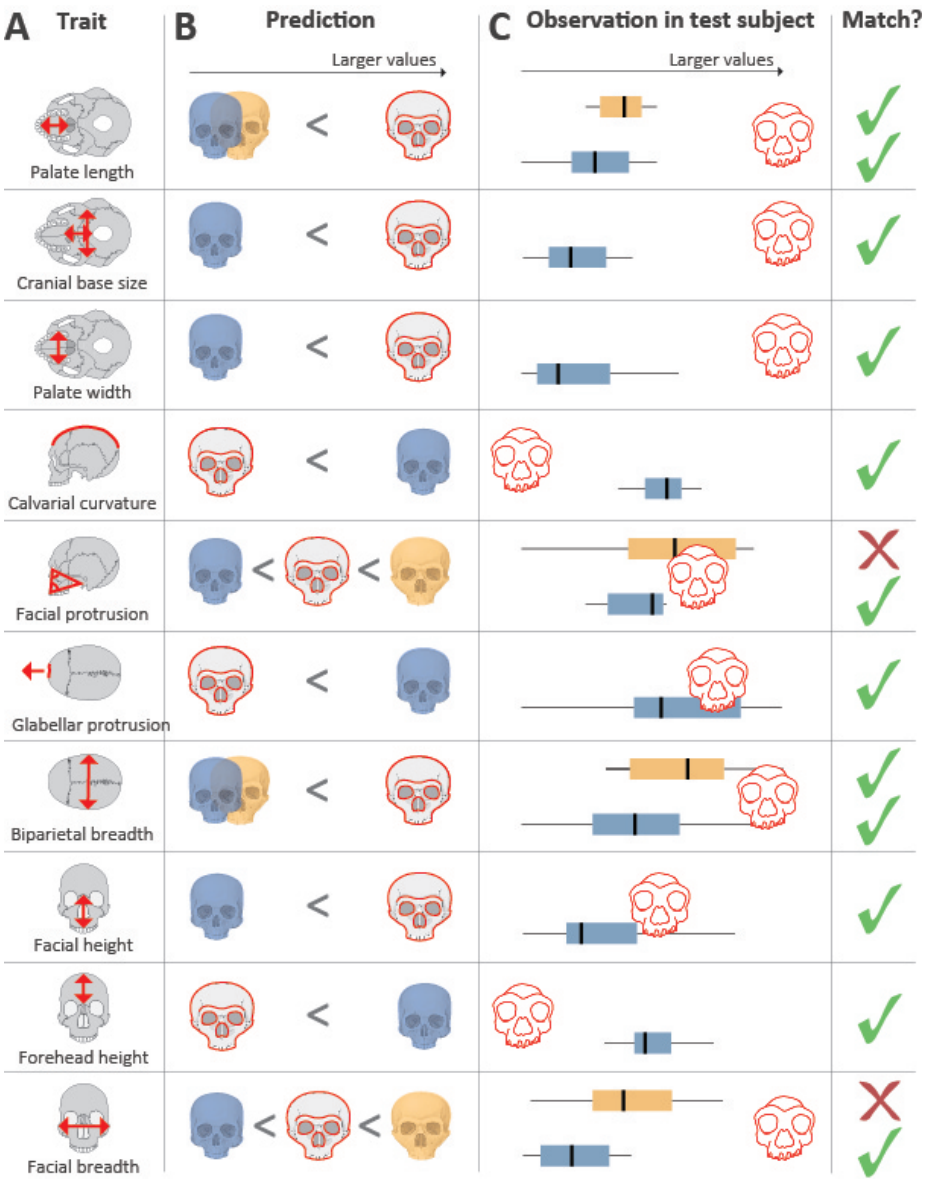

Figure 2: **A.** Measurements used to evaluate the match to the predicted Denisovan profile. **B.** Predicted relative value of the Denisovan (red outline) phenotype, compared to AMHs (blue) and Neanderthals (orange). **C.** Boxplots showing the distribution of each measurement in AMHs (blue) and Neanderthals (orange). The respective value of the Harbin cranium is presented as an example. Check and cross marks show whether the Harbin value matches the predicted Denisovan direction of difference.

3.2 Estimating the match between test subjects and the Denisovan profile

We estimate the degree of similarity of a specimen to the reconstructed Denisovan profile using a metric we refer to as the "d-distance" (a full description appears in the methods). The d-distance summarizes the measured quantiles with respect to the distribution of measured values in AMHs and Neanderthals. D-distance is scaled to the range $(-1, 1)$, with positive values reflecting agreement with the prediction in Denisovans, and negative values reflecting disagreement.

When measurements align with the Denisovan predicted profile, the d-distance is positive. Consequently, specimens resembling the Denisovan profile exhibit an asymmetric distribution skewed toward positive values (e.g., Fig. 3a). Conversely, specimens lacking resemblance to the Denisovan profile tend to display values that are either evenly dispersed or skewed toward negative values (e.g., Fig. 3b). It is important to note that a higher positive value does not necessarily mean a better fit to the Denisovan profile, as the directional predictions are qualitative and not quantitative. However, it does indicate increased confidence in the observed divergence between the test subject and the background population.

We first evaluated the match of each specimen to the predicted Denisovan profile by computing the fraction of positive NPDs for all measurements. The test subject achieving the highest d-distance fraction is Harbin (Fig. 3a) , displaying 12 out of 14 correct predictions. Conversely, an AMH specimen, Cro-Magnon II (Fig. 3b), exhibits the lowest ratio of 0 out of 9.

Overall, most test subjects show a higher fraction of positive d-distance compared to the background populations (Fig. 4). AMHs show match rates centered around half with a distribution close to normal. This is expected, as most predictions are relative to the AMH median. H. *erectus* specimens exhibit slightly higher match rates. Neanderthals present considerably higher match

rates, in line with their close phylogenetic relation to Denisovans and their high predicted morphological resemblance to Neanderthals [26].

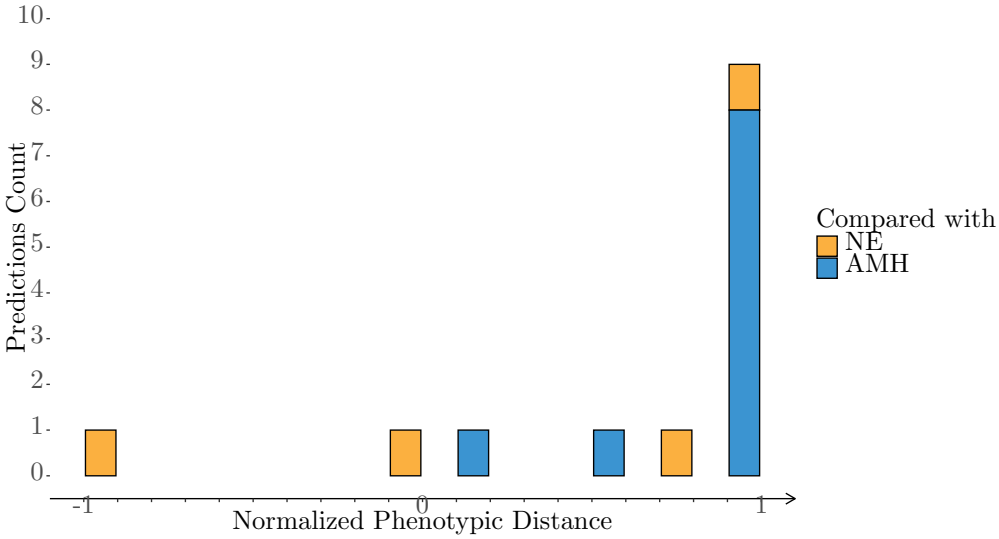

(a) Stacked histogram of d-distance values for the Harbin cranium (N =14). 12 Values in the positive range fall in line with the Denisovan predictions, while 2 fall in the negative range. The blue bars are predictions compared to AMHs, orange bars are compared to Neanderthals.

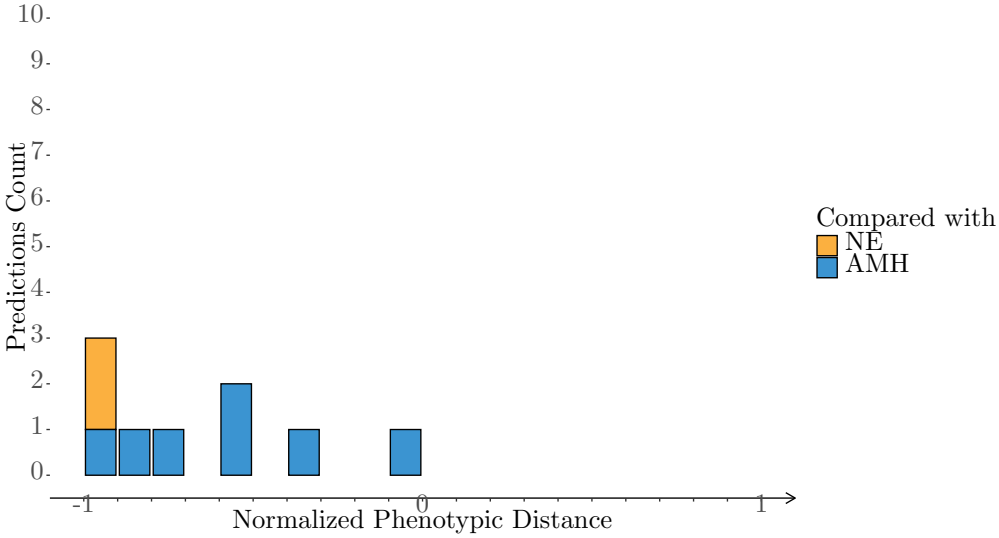

(b) Stacked histogram of d-distance values for the Cro-Magnon II cranium (N =9). All 9 values fall in the negative range, indicating very low fit to the Denisovan profile.

Figure 3: Overall match to the Denisovan profile represented as stacked histograms of d-distances.

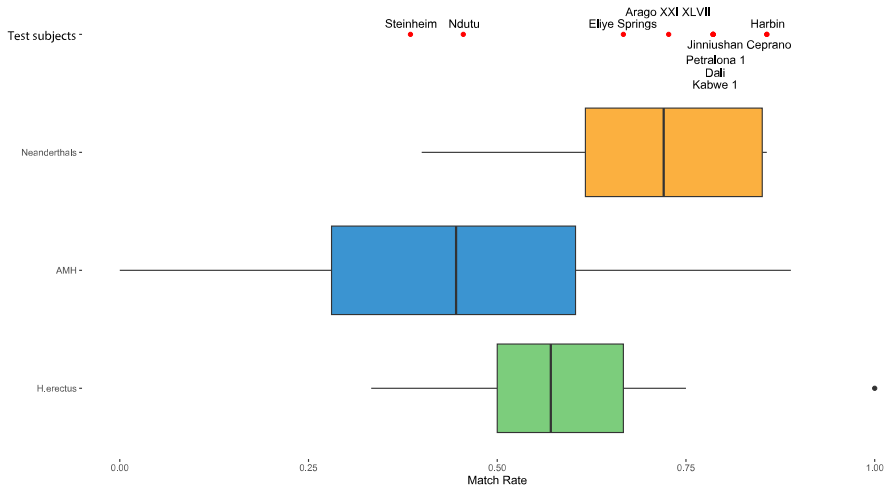

Figure 4: The test subjects' d-distance match rate compared to that of the the three established hominin groups included in the analsis

3.3 Harbin, Dali, and Kabwe are in high concordance with the Denisovan profile

We employed two strategies to evaluate the degree of concordance between each test subject and the predicted Denisovan profile. The first strategy investigated the proportion of comparisons matching the Denisovan profile. We found that the Harbin skull showed particularly high compatibility, with 12 out 14 comparisons matching predicted Denisovan traits (86%, Fig. 2C). This match rate is substantially higher than the observed rates in other hominin groups. Conducting the same test on Homo erectus, AMHs, and Neanderthals, yielded considerably lower match rates: 45% for AMHs, 59% for Homo erectus, and 70% for Neanderthals (Fig. 5). The relatively higher match rate of Neanderthals to the Denisovan profile likely stems from the close evolutionary proximity between these groups, resulting in many shared morphological characteristics. Indeed, the majority of predicted differences in the profile are between Denisovans and

AMHs rather than between Denisovans and Neanderthals [26].

The second strategy investigated the extent to which a test subject differs from AMHs and Neanderthals, and whether this difference is in the direction of the predicted Denisovan trait. Here we computed a score for each test subject using a Mann-Whitney U-test statistic. Thus, this approach assigned higher scores to crania that deviated more extremely in the direction of the predicted Denisovan trait across many traits. Dali and Kabwe ranked the highest when employing this method, closely followed by Harbin 6.

To further test how robust these matches are, and to account for potential correlations between traits, we employed permutation tests. We generated 1,000 random anatomical profiles, where each predicted Denisovan trait was randomly replaced with one of XXX cranial traits, while maintaining the number and directionality of predictions compared to each hominin group. Finally, we examined for each test subject how well it matches the Denisovan profile compared to random profiles. We found that correlations between traits cannot explain the resemblance of Harbin, Dali and Kabwe to the Denisovan profile, and that these skulls show a significantly better match to this profile than expected by chance (Dali: $P = 0.01$, Kabwe: $P = 0.02$, and Harbin: $P = 0.05$, permuted U-test, see Methods).

In summary, the Binomial statistic primarily focuses on the number of matches, while the U-test statistic additionally factors in the degree of extremity of the trait, giving more weight to more extreme differences between the test subject and the other groups. Nevertheless, because the exact extent of phenotypic change in Denisovans is unknown, it remains uncertain which approach better represents a match to the profile. Consequently, we utilized both methods to rank the specimens. Overall, three cranial specimens ranked consistently high in both methods: Harbin, Dali and Kabwe Fig. 5, 6.

The two scoring methods exhibit similarity with one another, as can be seen

in Fig 7.

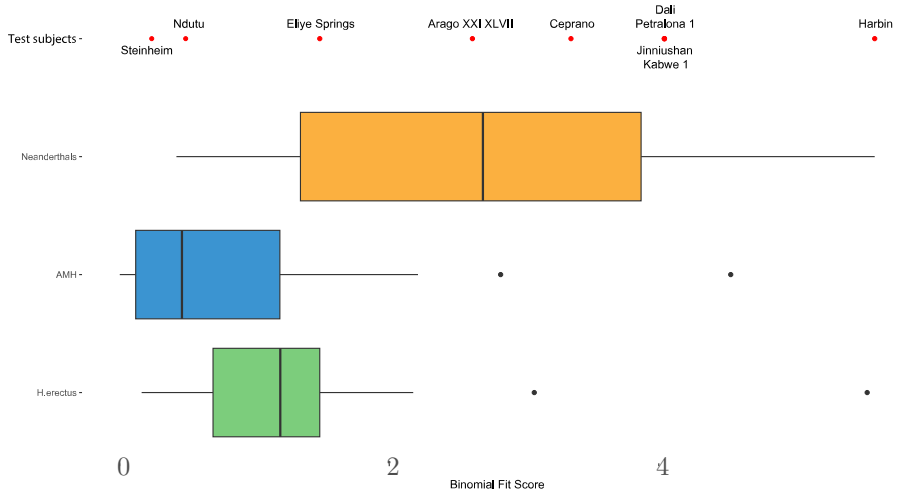

Figure 5: Test subject Binomial test match rates, compared to those of the the three background populations.

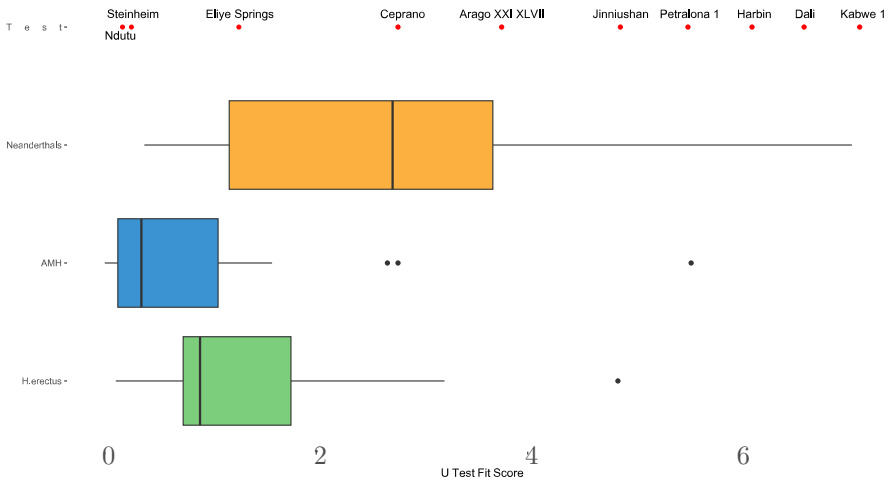

Figure 6: Test subject U-test scores compared to those of the background population.

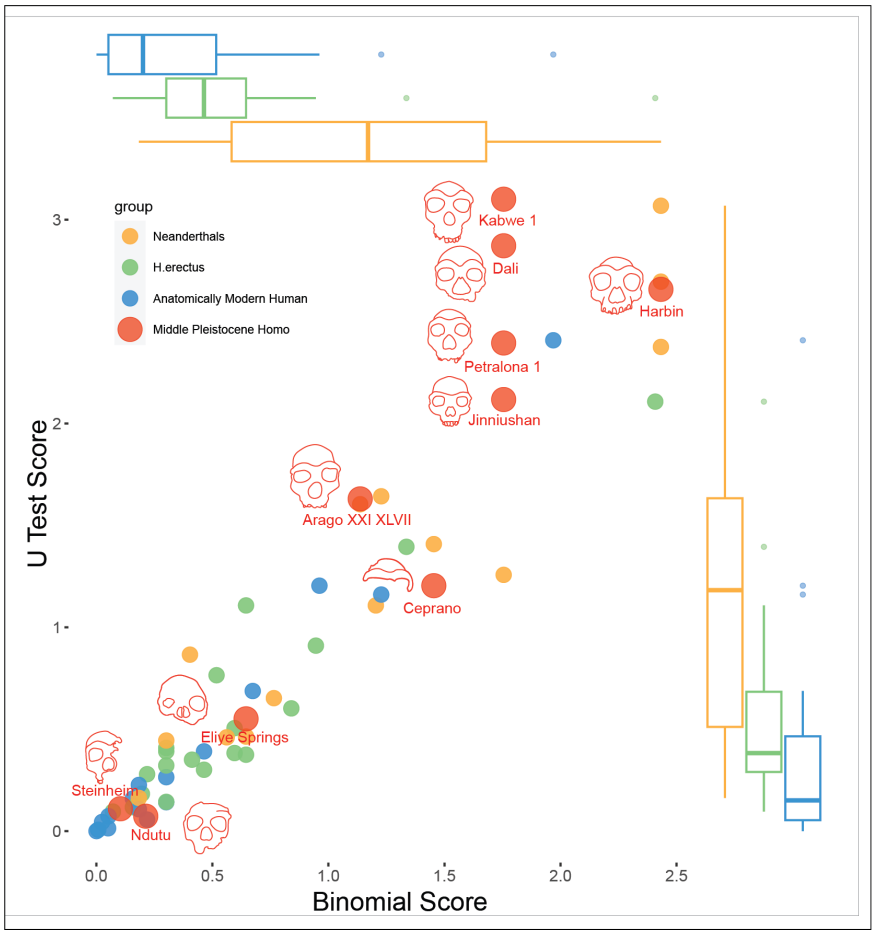

Figure 7: Dotplot combining the two score types (Binomial and U-test) for each specimen included in the analysis.

3.4 High scoring specimens exhibit morphological similarity

To explore potential morphological affinities between test subjects and examine if distinct clusters emerge, we carried out a PCA. The PCA included all available cranial metric measurements which had less than 20% missing data. After filtering the measurements 56 measurements were retained. Then we filtered

out specimens with more than 15% missing measurements were excluded from the analysis, to avoid over-imputation. As a result, 50 test subjects remained in the final PCA. To account for remaining missing data, we used the Singular Value Decomposition (SVD) method [31].

The PCA exhibited a high level of separation between the control groups: *Homo erectus*, Neanderthals and AMHs (Fig. 8). Notably, the three test specimens that displayed a high concordance with the Denisovan profile (Harbin, Dali, and Kabwe) clustered relatively close to one another in a clade that is mostly distinct from the other hominin lineages. This suggests that specimens resembling the Denisovan profile form a morphologically similar group, not only in their Denisovan-like traits. Moreover, PCA focusing solely on predicted, metric, and non-metric measurements (supplementary figures 6-7) exhibited similar clustering patterns and morphological relations between specimens, indicating that they are not merely a reflection of the overall cranial size.

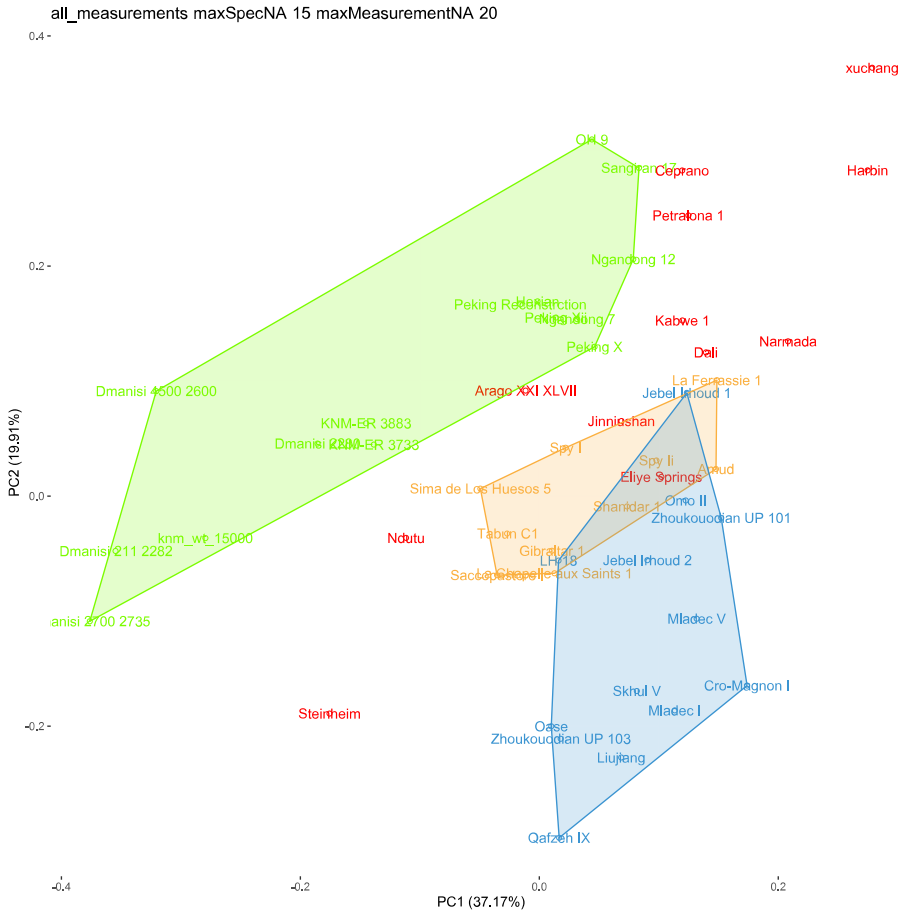

Figure 8: PCA of all specimens included in the analysis. the polygons represent the three background populations. High scored test subjects are clustered together, indicating on morphological similarity between them.

4 Methods

4.1 Selection of specimens

The majority of cranial measurements were directly taken from, or based on, the dataset provided by [16] in Morphobank [32] (project # 3385). Specimens in this dataset were excluded from the analysis if they:

1. Lacked a cranium
2. Pre-date the Neanderthal-Denisovan split (390-440 kya) [1]
3. Belong to a sub-adult
4. Have fewer than five testable predictions

In total we have 10 test subjects (debated Middle Pleistocene crania) 1. The comparison groups include 20 H. *erectus*, 18 H. *sapiens*, and 15 Neanderthal crania (supp. table 1).

We acknowledge that H. *floresiensis* and H. *luzonensis* share temporal and geographic overlap with the test subjects. However, they were not included in this study because they were absenct from the Morphobank dataset. Despite inhabiting Southeast Asia, their overall morphology and smaller dimensions strongly suggest that they represent distinct hominin lineages, differing significantly in anatomy from Denisovans. Similarly, we did not include H. *naledi* specimens in this study due to their distinct morphology, particularly their brain size, which likely places them on a separate hominin lineage from Denisovans [20].

4.2 Cranial Measurements

Predicted Denisovan phenotypes were taken from our original reconstruction [26] (supp table 6). Among the predictions in [26], we used only those which (1) can be matched with an available continuous measurement, and (2) have a directional prediction, namely those where the direction of change in the phenotype in Denisovans can be determined.

Each phenotype was associated with a continuous measurement based on its description in the Human Phenotype Ontology (HPO) database [33] and other sources of facial morphology (primarily [34]). For three predictions that did not have a corresponding continuous measurement (calvarial curvature, forehead height, and glabellar protrusion), we generated a fitting measure using available images from Ni *et al.* (2021) (see below).

Ni *et al.* (2021) provide two matrices in Morphobank: raw measurements (V1.0) and normalized measurements (v1.1). The normalized measurements were generated by dividing the raw measurements by the 1/3rd power of the cranial capacity of the respective specimen to account for the effect of body size. We decided to use the raw data for two reasons: First, the normalization method used by Ni *et al.* could create potential biases between the measurements of the neurocranium versus the viscerocranium. Ideally, the size would be calculated based on the centroid of the cranium 3D model, however these values were not provided. Second, almost all cranial phenotypes in the original reconstruction pointed at higher values in Denisovans, suggesting an overall increase in cranial size. Such cranial expansion could be missed using a normalized dataset.

It should be noted that the original reconstruction only used phenotypes where the prediction went through several quality control steps that assured high accuracy. One of these steps was to include in the list of Denisovan predictions only cases where methylation has been shown to be predictive of morphology in Neanderthals. In this respect, we acknowledge a mistake in our original

reconstruction, where we associated thicker enamel with Denisovans, failing to realize that our prediction of thicker enamel in Neanderthals was wrong in the first place. While Neanderthals were described to have a thicker layer of enamel compared to AMHs, their layer is in fact thinner on average [35]. Therefore, as in other traits where methylation was shown not to be predictive of morphology, we have removed this trait from the list of predictions used in the current work.

Below, we provide a detailed description of the predictions and their corresponding measurements (see also Supplementary Table S2).

4.2.1 Palate breadth

The Denisovan palate (roof of the mouth) is predicted to be wider than in AMHs based on the "Narrow palate" phenotype [HP:0000189]. This phenotype is described as decreased palatal width. Here, we measure it by the "maxilloalveolar breadth" (MAB), defined as the greatest breadth across the alveolar border, perpendicular to the medial plane [16].

4.2.2 Facial breadth

The Denisovan face is predicted to be wider than in AMHs and shorter than in Neanderthals based on the *small face* phenotype [HP:0000274] and the *Narrow face* phenotype [HP:0000275], which is hierarchically embedded within it. Here, we measure these phenotypes using the bizygomatic breadth (ZYB, zy-zy), similarly to previous measurements of the breadth of the upper face [34].

4.2.3 Facial height

The Denisovan face is predicted to be longer than in AMHs based on the *Short face* phenotype [HP:0011219], which is hierarchically embedded within the *Small*

face phenotype [HP:0000274]. This phenotype can be measured as the vertical distance between the nasion to the gnathion (the inferior border of the mandible) [34]. However, as the test subjects are missing a mandible, this measurement is unavailable. Instead, we used the upper facial height (NPH), defined as the vertical distance from the nasion to the prosthion.

4.2.4 Biparietal breadth

The Denisovan parietal bones are predicted to be more laterally expanded than in both AMHs and Neanderthals based on the "biparietal narrowing" phenotype [HP:0004422]. This is measured here by the "maximum biparietal breadth" measurement [16].

4.2.5 Cranial base area

Denisovans are predicted to have larger cranial base area than AMHs based on the "decreased cranial base ossification" phenotype [HP:0005451]. The cranial base is the supporting bony structure behind the midface (e.g., [36]). To estimate the cranial base size, we approximated it by the area of an ellipse with one axis measured by the "basion-nasion length" (BNL) and the other by the "biauricular breadth" (AUB). Therefore, $A_{\text{cranial base}} = \pi \times \text{AUB} \times \text{BNL}$, with both measurements taken from [16].

4.2.6 Dental arch length

Denisovans are predicted to have less crowded dental arches than both AMHs and Neanderhtals, based on the "dental crowding" phenotype [HP:0000678], described as an inadequate arch length for tooth size. Reduced dental crowding can be a result of three causes: (1) Increased length of the dental arch; (2) reduced number of teeth; or (3) smaller teeth. The dental formula of hominins

is highly consistent [37], making the second cause unlikely. The third cause is also unlikely, as the confirmed Denisovan teeth are much larger than in other *Homo* lineages [2]. We therefore concluded that the Denisovan dental arch is likely to be longer than in both AMHs and Neanderthals.

To test the dental arch length in the maxilla, we used the maxilloalveolar length, defined as the greatest length of the alveolar process of maxilla [16].

For the mandibular analysis of Xiahe we used the dental arcade length data taken from [9]. Data for all available Neanderthal groups (European and Asian Neanderthals) was combined. Data for all AMH groups (Early H. *sapiens*, Late Pleistocene H. *sapiens*, Late Pleistocene Asian H. *sapiens*) were also combined.

4.2.7 Facial protrusion

Denisovans are predicted to have greater facial protrusion than in AMHs, but lower than in Neanderthals, based on the "flat face" phenotype [HP:0012368]. The convexity (or concavity) of the face is examined in profile view [34].

To measure facial protrusion, we used the nasion angle (NAA) and prosthion angle (PRA). Both measurements are used as measures of prognathism [16]. Since these angels were not provided in the database, we generated them using the law of cosines and the relevant facial measurements which were provided (NPH, BNL, BPL).

The two measurements (PRA, NAA) were combined into a single value - the protrusion index, defined as the first principal component. This component explains 94% of the variability in the two measurements.

We preferred to use PCA rather than linear regression, as the latter assumes asymmterical dependency between the variables, whereas in reality the dependency between the variables is symmetrical.

4.2.8 Measurements based on cranial images

The procedures for calculating calvarial flatness, forehead height and glabellar protrusion were applied to images of the crania which are assumed to be consistently positioned in standard anatomical position following the Frankfurt planes. Images were provided in JPEG format in RGB or grayscale color-space. All images underwent a vectorization procedure, converting each non-white pixel into (x, y) coordinates. Pixels were considered white if the magnitude of the difference vector between their RGB values and standard white $(255, 255, 255)$ was smaller than 20. The skull boundary was extracted using the Matlab alpha shape boundary algorithm with a 0.9 shrink factor. This provided an ordered list of points $(x_i, y_i), i = 1 \ldots N$ on the closed curve forming the outer boundary of the cranium.

This closed curve is then expressed in term of a series of Fourier coefficients [38]. As the cranium boundary is continuous, the coordinates of each vertex in each of the two dimensions can be thought of as a unique function of the arc-length denoted as s, with $0 \leq s \leq L$, where $L = \sum_{i=1}^{N-1} \sqrt{(x_{i+1} - x_i)^2 + (y_{i+1} - y_i)^2}$. As N must be an even number for the subsequent procedure, in case it is odd one vertex is removed. For convenience, the vertices are shifted by interpolation along the curve so that the distance between each two points will be constant. A discrete Fourier series is then fitted onto the points $x(s), y(s) = \sum_n (A_n^{x,y} \sin\left(\frac{2\pi n}{L} s\right) + B_n^{x,y} \cos\left(\frac{2\pi n}{L} s\right))$, with $n = 0, \ldots, \frac{N}{2}$ for each dimension (x, y). The fitting is performed by solving a system of linear equations through matrix inversion. This provides a list of Fourier coefficients (A_n, B_n) for each of the two dimensions which allow to express the coordinates of the curve for each arc-length value.

The maximal resolution in which the curve can be expressed equals to the shortest wavelength of the Fourier series $\frac{2L}{N}$. However, for some applications such as finding prominent low-level features such as locations of curvature peaks

it is sometimes useful to reduce the curves resolution. This is achieved by introducing a smoothing factor [38] that provides a weight to each term in the series $x(s), y(s) = \sum_n w_n \left(A_n^{x,y} \sin\left(\frac{2\pi n}{L} s\right) + B_n^{x,y} \cos\left(\frac{2\pi n}{L} s\right)\right)$ where $w_n = \frac{1}{1+e^{\frac{n-N_{\text{eff}}}{\Delta}}}$. N_{eff} is a constant value chosen to reflect the number of terms in the series to be considered as $w_n \approx 1$ for $n < N_{\text{eff}}$ and $w_n \to 0$ as n increases beyond it where Δ reflects an interval over which this transition gradually occurs.

The Fourier series which allows to express the (x, y) coordinates as a function of arc-length s can be differentiated [38]. Its first derivative is used to expresses the tangent angle as a function of the arc-length $T(s) = \tan^{-1} \frac{y'(s)}{x'(s)}$. Its second derivative is used to express the curvature as a function of the arc-length $C(s) = -\frac{y'x''-x'y''}{x'^2+y'^2}$.

4.2.9 Calvarial curvature

Denisovans are predicted to have a calvarium (top of the cranium) which is flatter in lateral view than in AMHs, based on the "oxycephaly" phenotype [HP:0000263].

Here, we measure the calvarial curvature using a lateral image of the cranium. The anterior boundary of the cranial top is set to be the supraoribtal suclus, defined as a local negative minimum of the curvature function. The posterior boundary is set to be the mirror reflected projection of the supraoribtal suclus on the posterior part of the cranium. This point could have been identified automatically from the curvature function. However, many the crania are fragmented in different ways, which prevent an anatomically consistent choice. To avoid such errors, a semi-automatic approach was used in which the analyst selects the correct critical points out of several potential points within a graphical user interface (Supplementary Fig. 1). The potential points are all those for which there is a local negative minimum in the curvature function and whose x coordinate is positive, as the critical point is concave and anteriorly positioned.

The identification of the local minima is done iteratively with $N_{eff} = 15$ in the first round, allowing to identify only low-level features and filter out points generated due to noise. The exact arc-length value of the points identified in the first round is then refined using a higher value of $N_{eff} = 45$ allowing to accurately identify their position.

Once the critical point is selected the arc-length values corresponding to the superior cranial curve segment are plugged in to the function to calculate 100 equidistant points on the curve under low smoothing with N_{eff} equal to 80% of the number of terms in the Fourier series. These points are then scaled to centroid size $CS = \sqrt{\sum_{i=1}^{n} ((x_i - \bar{x})^2 + (y_i - \bar{y})^2)}$ corresponding to the mean of all points on the curve. The scaled curve segment points are then fitted with the function $x(s), y(s) = A^{(x,y)} \cos\left(\frac{s}{L}\right) + B^{(x,y)} \sin\left(\frac{s}{L}\right) + C^{(x,y)} \left(\cos\left(\frac{s}{L}\right)\right)^3 + D^{(x,y)} \left(\sin\left(\frac{s}{L}\right)\right)^3$ by solving an overdetermined system of linear equations. This function was chosen due to the balance it provides between compactness and error rates, allowing to express the general morphological aspect of the top of the skull while smoothing local irregularities which may result from post depositional damage. Similarly to the Fourier series, this function too is differentiated twice to calculate the tangent and curvature as function of arc length expressing the angle between the tangent to the curve at its curvature.

The flatness of the top of the cranium is calculated as the integral of the curvature's absolute value over the curve segment representing the top of the cranium to provide the cranial flatness value $CF = \int_{\theta_0}^{\theta_r} |C(s)| \, d\theta$ with s_r being the critical point's posterior reflection, such that lower values reflect a flatter segment (Supplementary Fig. 2 - 3).

4.2.10 Forehead height

Denisovans are predicted to have a lower forehead than AMHs based on the "high forehead" phenotype [HP:0000348].

Similarly to the calculation of the calvarial curvature, here we also use lateral image of the cranium. The cranial top is defined as described for the calvarial curvature, then the tangent function is used to identify the cranial vertex as at that point $T(s) = 0$. It is also used to locate the forehead point, which has been arbitrarily defined as $T(s_{fr}) = \pi/4$ between the critical point and the cranial vertex. This allows calculating the forehead height $FH = y(s_{fr}) - y(s_0)$ with s_0 being the critical point.

4.2.11 Glabellar protrusion

Denisovans are predicted to have a retracted glabella compared to AMHs. This phenotype was not present in the published reconstruction [26], due to being incorrectly labeled as a false prediction in Neanderthals. The phenotype was initially interpreted as the absolute protrusion of the glabella, as part of the supraorbital tours. However, after a re-evaluation we concluded that the phenotype was initially misinterpreted. The glabellar protrusion refers to the relative protrusion of the midsagittal area of the foreahead, relatively to the rest of the supraorbital ridges [34]. Since Neanderthals indeed have a relatively retracted glabella, the status of the predictions was changed to correct.

Here, we measure the relative protrusion of the glabella using superior images of the cranium. For this measurement we only used crania which have an intact supra orbital torus in the midsagittal plane. In cases where the midfacial bones were apparent in superior view they were digitally removed. This procedure was done for the following specimens: Sima de los huesos 5, Dmanisi 2282,Dmanisi 2700, Saccopastore 1 and Shanidar 5.

A similar procedure is also used to express the glabellar curvature on superior view images in which the anterior end of the cranium is facing right (Supplementary Fig. 4). Here too it is assumed that all crania are presented in an anatomical position. The boundary of the cranium and its Fourier coef-

ficients representation are extracted using the same procedure detailed above with smoothing factor $N_eff = 20$. Given the cranial morphology, the boundary curve centering and the assumption of consistent rotation, the arc-length value of the glabella s_{gl} is that for which $fx(s_{gl}) > 0, fy(s_{gl}) = 0$. Thus the glabellar region is defined as the segment of the curve ranging between $s_{gl} \pm \frac{L}{25}$ (Supplementary Fig. 5). Within this section the value of the curvature function was calculated for s_{gl} as well as for other 20 equidistant points within the region. The glabellar curvature is expressed as $C(s_{gl})$. In cases where there was a noticeable cranial asymmetry which prevented s_{gl} from corresponding to the anatomical glabella, the value of the correct point was selected manually by the analyst out of the 20 points for which the curvature value was calculated.

4.3 Percentile estimation

Each single comparison is carrying out by computing the percentile of a particular measurement in a particular test subject within the distribution of this measurement in a reference group (either Neanderthals or AMHs).

To this end, let t be the value of the measurement in the test subject, and let $t_1 \leq t_2 \leq \ldots \leq t_N$ be its values in the reference group. Then, the percentile is computed following these steps: (1) Outliers are removed from the reference group. (2) The value t_i in the reference group is taken as the estimator of the quantile$q_i = \frac{i-0.5}{N}$. (3) The remaining quantiles are then linearly interpolated using the approxfun function, to create a cumulative distribution function (CDF). (4) The quantile of tied values is taken as the mean of the respective quantiles (the parameter 'ties' is set to 'mean'). (5) the percentile of t would be estimated based the generated group cumulative distribution function (CDF).

4.4 D-distance

Quantiles were then transformed into a value we call the "D distance". It reflects the normalized phenotypic distance of an test subject from the predicted Denisovan profile by accounting for the predicted direction of change in Denisovans for each measurement. D distance is scaled to the range $(-1, 1)$, with positive values reflecting agreement with the prediction in Denisovans, and negative values reflecting disagreement. To this end, quantiles are first centered around 0 by subtracting 0.5. Then, we account for the predicted direction of change by flipping the sign if the prediction is that the measurement in Denisovans is lower than in the background population. Finally, we scale the distance by multiplying by two. Let s be +1 if the prediction is the the measurement would be higher in Denisovans, and -1 if it is the other way around. Let q be the quantile of the measurement in a specific specimen compared to the histogram of the background population. Then, the d Distance is

$$d = 2s\left(q - \frac{1}{2}\right).$$

When measurements align with the Denisovan predicted profile, the d Distance is positive. Consequently, specimens resembling the Denisovan profile exhibit an asymmetric distribution skewed toward positive values (e.g., Fig. 3a). Conversely, specimens lacking resemblance to the Denisovan profile tend to display values that are either evenly dispersed or skewed toward negative values (e.g., Fig. 3b). It is important to note that a higher positive value does not necessarily mean a better fit to the Denisovan profile, as the directional predictions are qualitative and not quantitative. However, it does indicate increased confidence in the observed divergence between the test subject and the background population.

4.5 Scoring the match between a test subject and the Denisovan profile

Let $d_1, d_2, \ldots, d_k$ be the d-distances obtained for a particular test subject. Based on these distances, we scored how closely the test specimen resembles the predicted Denisovan profile using two approaches. First, we used one-tailed Wilcoxon signed-rank test to compare the d-distances to zero. This was implemented using the wilcoxsign_test function from the 'coin' package [39]. We used this function instead of the base one in R since its implementation of the test accepts tied values. Second, we considered the prediction as correct if the corresponding d-distance was greater than zero. Then, we used a one-tailed binomial test, calculated using the 'binom.test' function in R with continuity correction [40, 41].

The P-values generated by both tests were then corrected for multiple comparisons using the Benjamini-Hochberg method, implemented in the p.adjust method. Importantly, only the test subjects were accounted for multiple comparisons, as all other specimens were not tested for their resemblance with the Denisovan profile.

The facial features examined in this work are highly correlated, which violate the assumption of both statistical tests. Hence, we do not assign statistical meaning to the P-values, but rather treat them as scores which indicate the relative similarity of each specimen to the Denisovan profile. The scores are calculates for both statistical test as

$$\text{Score} = -log(\text{P} - \text{val})$$

4.6 Principal Component Analysis

Since most crania used in the analysis are incomplete, many measurements were missing. To compute PCA, missing data had to be imputed. To this end, we used the 'missMDA' package [31]. This package imputes missing data by iterative PCA, which takes into account the correlation between variables and similarity between instances. Values were imputed using the function 'imputePCA' with default parameters: scaled data and two dimensions.

To avoid over-imputation of the data, we first filtered out measurements with over 20% missing values, and then specimens with more than 15% missing values. These values were selected in order to keep a maximum amount of specimens while still keeping imputation low.

In addition to the main PCA, we also computed separate PCAs for the metric measurements and the non-metric measurements (e.g., angles, ratio). Since there are fewer non-metric measurements available, we increased the missing measurement threshold to 70% in order to retain more dimensions. The specimen missing values threshold is remains 15%. As a result, the overall imputation remains the same, but with fewer specimens being kept in the non-metric PCA.

PCA was computed based on the reference groups, and the test subjects were later projected onto this plane to produce the final plot.

5 Discussion

Identifying Denisovans in the fossil record is a key step to understanding their evolution. However, this is a highly challenging task, as attested by the scarcity of confirmed Denisovan specimens. Here, we proposed that reconstructing Denisovan morphology using gene regulatory patterns provides a promising link between Denisovan genetics and anatomy, allowing for testing the resemblence of many specimens to the predicted Denisovan anatomical profile. We assessed the compatibility of Middle Pleistocene hominin specimens with the Denisovan skeletal reconstruction [26]. Three specimens have displayed notably high scores, indicating a good resemblance to the Denisovan profile: Harbin, Dali, and Kabwe. Two of these, Harbin and Dali, have previously been suggested to share connections with Denisovans, either through circumstantial evidence (e.g., their temporal and geographical context) or through some morphological similarities to the few confirmed Denisovan features [25, 1]. Our results provide a systematic scan of debated or unclassified specimens and suggest that these three individuals are possibly Denisovans or their close relatives.

Almost all AMH and H. *erectus* specimens we tested received relatively low scores, indicating that the test is not universally permissive, and that lineages that are relatively far from Denisovans do not tend to align with the profile. Neanderthals, which are expected to share many traits with Denisovans (based both on their phylogeny as well as our reconstructed profile), tend to show higher scores than AMHs and H. *erectus*. However, even within Neanderthals, only two specimens received scores as high as Harbin, Dali, and Kabwe (Fig. 3). Overall, the rare occurrence of false positives (high-scoring non-Denisovan specimens), the >85% accuracy in predicting chimpanzee and Neanderthal phenotypes, and the observation that later confirmed Denisovan specimen confirmed the majority of our predictions [9], support the robustness of this method in detecting Denisovan-like morphologies.

The resemblance of the Denisovan profile to several H. *heidelbergensis* specimens, and specifically the African specimen from Kabwe, is particularly intriguing. Despite our limited understanding of the true range of Denisovans, it is unlikely that they reached Southern Africa. A more likely explanation is that the resemblance of some H. *heidelbergensis* specimens to the Denisovan profile reflects the proposed phylogenetic position of H. heidelbergensis either close to the split between modern humans and archaic humans or close to that between Neanderthals and Denisovans. If H. *heidelbergensis* is indeed phylogenetically close to the Neanderthal-Denisovan divergence, it is expected to exhibit even greater similarity to the Denisovan profile than the similarly of Neanderthals to the profile. An alternative explanation is that Denisovans possibly retained several ancestral morphologies observed in H. heidelbergensis [42].

6 Acknowledgements

D.G. was supported by the Center for New Scientists at the Weizmann Institute of Science and the Kahn Family Research Center for Systems Biology of the Human Cell.

6.1 G.H. and U.S

6.1.1 General

The Computational Archaeology Laboratory, The Institute of Archaeology, The Hebrew University of Jerusalem

6.1.2 Funding

The department of Physics of Complex Systems, Weizmann Institute of Science The Braginsky Center for the Interface between Science and the Humanities, Weizmann Institute of Science The Israel Science Foundation Grant No. 1745/21 granted to Uzy Smilansky The Israel Academy of Science and Humanities Postodctoral Fellowship Granted to Gadi Herzlinger

We would like to thank Chris Stringer, Erella Hovers, and Anna Belfer-Cohen for useful advice and feedback.

7 Bibliography

References

[1] Stéphane Peyrégne, Viviane Slon, and Janet Kelso. "More than a decade of genetic research on the Denisovans". en. In: *Nature Reviews Genetics* (Sept. 2023). Publisher: Nature Publishing Group, pp. 1–21. ISSN: 1471-0064. DOI: 10.1038/s41576-023-00643-4. URL: https://www.nature.com/articles/s41576-023-00643-4 (visited on 01/01/2024).

[2] David Reich et al. "Genetic history of an archaic hominin group from Denisova Cave in Siberia". en. In: *Nature* 468.7327 (Dec. 2010). Number: 7327 Publisher: Nature Publishing Group, pp. 1053–1060. ISSN: 1476-4687. DOI: 10.1038/nature09710. URL: https://www.nature.com/articles/nature09710 (visited on 01/05/2024).

[3] Viviane Slon et al. "A fourth Denisovan individual". In: *Science Advances* 3.7 (July 2017). Publisher: American Association for the Advancement of Science, e1700186. DOI: 10.1126/sciadv.1700186. URL: https://www.science.org/doi/10.1126/sciadv.1700186 (visited on 01/05/2024).

[4] Fabrizio Mafessoni et al. "A high-coverage Neandertal genome from Chagyrskaya Cave". In: *Proceedings of the National Academy of Sciences* 117.26 (June 2020). Publisher: Proceedings of the National Academy of Sciences, pp. 15132–15136. DOI: 10.1073/pnas.2004944117. URL: https://www.pnas.org/doi/10.1073/pnas.2004944117 (visited on 12/31/2023).

[5] Susanna Sawyer et al. "Nuclear and mitochondrial DNA sequences from two Denisovan individuals". In: *Proceedings of the National Academy of Sciences* 112.51 (Dec. 2015). Publisher: Proceedings of the National Academy of Sciences, pp. 15696–15700. DOI: 10.1073/pnas.1519905112. URL: https://www.pnas.org/doi/full/10.1073/pnas.1519905112 (visited on 04/07/2024).

[6] Dongju Zhang et al. "Denisovan DNA in Late Pleistocene sediments from Baishiya Karst Cave on the Tibetan Plateau". In: *Science* 370.6516 (Oct. 2020). Publisher: American Association for the Advancement of Science, pp. 584–587. DOI: 10.1126/science.abb6320. URL: https://www.science.org/doi/10.1126/science.abb6320 (visited on 02/10/2024).

[7] Samantha Brown et al. "The earliest Denisovans and their cultural adaptation". In: *Nature ecology & evolution* 6.1 (Jan. 2022), pp. 28–35. ISSN: 2397-334X. DOI: 10.1038/s41559-021-01581-2. URL: https://www.ncbi.nlm.nih.gov/pmc/articles/PMC7612221/ (visited on 04/07/2024).

[8] E. Andrew Bennett et al. "Morphology of the Denisovan phalanx closer to modern humans than to Neanderthals". In: *Science Advances* 5.9 (Sept. 2019), eaaw3950. ISSN: 2375-2548. DOI: 10.1126/sciadv.aaw3950. URL: https://www.ncbi.nlm.nih.gov/pmc/articles/PMC6726440/ (visited on 04/18/2024).

[9] Fahu Chen et al. "A late Middle Pleistocene Denisovan mandible from the Tibetan Plateau". en. In: *Nature* 569.7756 (May 2019). Number: 7756 Publisher: Nature Publishing Group, pp. 409–412. ISSN: 1476-4687. DOI: 10.1038/s41586-019-1139-x. URL: https://www.nature.com/articles/s41586-019-1139-x (visited on 01/05/2024).

[10] Fabrice Demeter et al. "A Middle Pleistocene Denisovan molar from the Annamite Chain of northern Laos". en. In: *Nature Communications* 13.1 (May 2022). Publisher: Nature Publishing Group, p. 2557. ISSN: 2041-1723. DOI: 10.1038/s41467-022-29923-z. URL: https://www.nature.com/articles/s41467-022-29923-z (visited on 04/18/2024).

[11] Chun-Hsiang Chang et al. "The first archaic Homo from Taiwan". en. In: *Nature Communications* 6.1 (Jan. 2015). Number: 1 Publisher: Nature Publishing Group, p. 6037. ISSN: 2041-1723. DOI: 10.1038/ncomms7037. URL: https://www.nature.com/articles/ncomms7037 (visited on 02/10/2024).

[12] A. Ascenzi et al. "A calvarium of lateHomo erectusfrom Ceprano, Italy". In: *Journal of Human Evolution* 31.5 (Nov. 1996), pp. 409–423. ISSN: 0047-2484. DOI: 10.1006/jhev.1996.0069. URL: https://www.sciencedirect.com/science/article/pii/S004724849690069X (visited on 04/10/2024).

[13] A. Ascenzi et al. "A re-appraisal of Ceprano calvaria affinities with Homo erectus, after the new reconstruction". In: *Journal of Human Evolution* 39.4 (Oct. 2000), pp. 443–450. ISSN: 0047-2484. DOI: 10.1006/jhev.2000.0425. URL: https://www.sciencedirect.com/science/article/pii/S0047248400904251 (visited on 04/10/2024).

[14] Glenn C. Conroy et al. "Newly discovered fossil hominid skull from the Afar depression, Ethiopia". en. In: *Nature* 276.5683 (Nov. 1978). Publisher: Nature Publishing Group, pp. 67–70. ISSN: 1476-4687. DOI: 10.1038/276067a0. URL: https://www.nature.com/articles/276067a0 (visited on 04/10/2024).

[15] Christopher J. Bae et al. "Moving away from "the Muddle in the Middle" toward solving the Chibanian puzzle". en. In: *Evolutionary Anthropology: Issues, News, and Reviews* n/a.n/a (). _eprint: https://onlinelibrary.wiley.com/doi/pdf/10.1002/evan.2201 e22011. ISSN: 1520-6505. DOI: 10.1002/evan.22011. URL: https://onlinelibrary.wiley.com/doi/abs/10.1002/evan.22011 (visited on 01/09/2024).

[16] Xijun Ni et al. "Massive cranium from Harbin in northeastern China establishes a new Middle Pleistocene human lineage". In: *The Innovation* 2.3 (Aug. 2021), p. 100130. ISSN: 2666-6758. DOI: 10.1016/j.xinn.2021.100130. URL: https://www.sciencedirect.com/science/article/pii/S2666675821000552 (visited on 01/01/2024).

[17] Xinzhi Wu and Sheela Athreya. "A description of the geological context, discrete traits, and linear morphometrics of the Middle Pleistocene hominin from Dali, Shaanxi Province, China". en. In: *American Journal of Physical Anthropology* 150.1 (2013). _eprint: https://onlinelibrary.wiley.com/doi/pdf/10.1002/ajpa.22188, pp. 141–157. ISSN: 1096-8644. DOI: 10.1002/ajpa.22188. URL: https://onlinelibrary.wiley.com/doi/abs/10.1002/ajpa.22188 (visited on 04/07/2024).

[18] Karen R. Rosenberg, Lü Zuné, and Christopher B. Ruff. "Body size, body proportions, and encephalization in a Middle Pleistocene archaic human from northern China". In: *Proceedings of the National Academy of Sciences* 103.10 (Mar. 2006). Publisher: Proceedings of the National Academy of Sciences, pp. 3552–3556. DOI: 10.1073/pnas.0508681103. URL: https://www.pnas.org/doi/full/10.1073/pnas.0508681103 (visited on 04/13/2024).

[19] Zhan-Yang Li et al. "Late Pleistocene archaic human crania from Xuchang, China". In: *Science* 355.6328 (Mar. 2017). Publisher: American Association for the Advancement of Science, pp. 969–972. DOI: 10.1126/science.aal2482. URL: https://www.science.org/doi/10.1126/science.aal2482 (visited on 04/07/2024).

[20] Xiu-Jie Wu et al. "Evolution of cranial capacity revisited: A view from the late Middle Pleistocene cranium from Xujiayao, China". In: *Journal of Human Evolution* 163 (Feb. 2022), p. 103119. ISSN: 0047-2484. DOI: 10.1016/j.jhevol.2021.103119. URL: https://www.sciencedirect.com/science/article/pii/S0047248421001718 (visited on 04/11/2024).

[21] Xiu-Jie Wu et al. "Archaic human remains from Hualongdong, China, and Middle Pleistocene human continuity and variation". In: *Proceedings of the National Academy of Sciences* 116.20 (May 2019). Publisher: Proceedings of the National Academy of Sciences, pp. 9820–9824. DOI: 10.1073/pnas.1902396116. URL: https://www.pnas.org/doi/full/10.1073/pnas.1902396116 (visited on 04/09/2024).

[22] Christopher J. Bae et al. ""Dragon man" prompts rethinking of Middle Pleistocene hominin systematics in Asia". In: *The Innovation* 4.6 (Oct. 2023), p. 100527. ISSN: 2666-6758. DOI: 10.1016/j.xinn.2023.100527. URL: https://www.ncbi.nlm.nih.gov/pmc/articles/PMC10661591/ (visited on 01/05/2024).

[23] G. Philip Rightmire. "Brain size and encephalization in early to Mid-Pleistocene Homo". en. In: *American Journal of Physical Anthropology* 124.2 (2004). _eprint: https://onlinelibrary.wiley.com/doi/pdf/10.1002/ajpa.10346, pp. 109–123. ISSN: 1096-8644. DOI: 10.1002/ajpa.10346. URL: https://onlinelibrary.wiley.com/doi/abs/10.1002/ajpa.10346 (visited on 01/05/2024).

[24] Xing Gao et al. "Revisiting the origin of modern humans in China and its implications for global human evolution". en. In: *Science China Earth Sciences* 53.12 (Dec. 2010), pp. 1927–1940. ISSN: 1869-1897. DOI: 10.1007/s11430-010-4099-4. URL: https://doi.org/10.1007/s11430-010-4099-4 (visited on 01/05/2024).

[25] Chris Stringer. "The status of Homo heidelbergensis (Schoetensack 1908)". en. In: *Evolutionary Anthropology: Issues, News, and Reviews* 21.3 (2012). _eprint: https://onlinelibrary.wiley.com/doi/pdf/10.1002/evan.21311, pp. 101–107. ISSN: 1520-6505. DOI: 10.1002/evan.21311. URL: https://onlinelibrary.wiley.com/doi/abs/10.1002/evan.21311 (visited on 01/01/2024).

[26] David Gokhman et al. "Reconstructing Denisovan Anatomy Using DNA Methylation Maps". In: *Cell* 179.1 (Sept. 2019), 180–192.e10. ISSN: 0092-8674. DOI: 10.1016/j.cell.2019.08.035. URL: https://www.

sciencedirect.com/science/article/pii/S0092867419309547 (visited on 01/16/2024).

[27] David Gokhman et al. "Reconstructing the DNA Methylation Maps of the Neandertal and the Denisovan". In: *Science* 344.6183 (May 2014). Publisher: American Association for the Advancement of Science, pp. 523–527. DOI: 10.1126/science.1250368. URL: https://www.science.org/doi/10.1126/science.1250368 (visited on 01/29/2024).

[28] David Gokhman et al. "Differential DNA methylation of vocal and facial anatomy genes in modern humans". en. In: *Nature Communications* 11.1 (Mar. 2020). Number: 1 Publisher: Nature Publishing Group, p. 1189. ISSN: 2041-1723. DOI: 10.1038/s41467-020-15020-6. URL: https://www.nature.com/articles/s41467-020-15020-6 (visited on 01/29/2024).

[29] Matthias Meyer et al. "A mitochondrial genome sequence of a hominin from Sima de los Huesos". en. In: *Nature* 505.7483 (Jan. 2014). Publisher: Nature Publishing Group, pp. 403–406. ISSN: 1476-4687. DOI: 10.1038/nature12788. URL: https://www.nature.com/articles/nature12788 (visited on 04/12/2024).

[30] Fabio Di Vincenzo et al. "Digital reconstruction of the Ceprano calvarium (Italy), and implications for its interpretation". en. In: *Scientific Reports* 7.1 (Oct. 2017). Publisher: Nature Publishing Group, p. 13974. ISSN: 2045-2322. DOI: 10.1038/s41598-017-14437-2. URL: https://www.nature.com/articles/s41598-017-14437-2 (visited on 04/18/2024).

[31] Julie Josse and François Husson. "**missMDA** : A Package for Handling Missing Values in Multivariate Data Analysis". en. In: *Journal of Statistical Software* 70.1 (2016). ISSN: 1548-7660. DOI: 10.18637/jss.v070.i01. URL: http://www.jstatsoft.org/v70/i01/ (visited on 02/16/2024).

[32] (MA) (O'Leary) and (SG) (Kaufman). *MorphoBank 3.0: Web application for morphological phylogenetics and taxonomy. 2012*. 2016. URL: http://www.%20morphobank.%20org.

[33] Sebastian Köhler et al. "The Human Phenotype Ontology in 2021". In: *Nucleic Acids Research* 49.D1 (Dec. 2020), pp. D1207–D1217. ISSN: 0305-1048. DOI: 10.1093/nar/gkaa1043. URL: https://www.ncbi.nlm.nih.gov/pmc/articles/PMC7778952/ (visited on 02/27/2024).

[34] Judith E. Allanson et al. "Elements of Morphology: Standard Terminology for the Head and Face". In: *American journal of medical genetics. Part A* 149A.1 (Jan. 2009), pp. 6–28. ISSN: 1552-4825. DOI: 10.1002/ajmg.a.32612. URL: https://www.ncbi.nlm.nih.gov/pmc/articles/PMC2778021/ (visited on 02/27/2024).

[35] Anthony J. Olejniczak et al. "Dental tissue proportions and enamel thickness in Neandertal and modern human molars". In: *Journal of Human Evolution* 55.1 (July 2008), pp. 12–23. ISSN: 0047-2484. DOI: 10.1016/j.jhevol.2007.11.004. URL: https://www.sciencedirect.com/science/article/pii/S0047248408000031 (visited on 04/02/2024).

[36] Xiu-Ping Wu et al. "Morphological Characteristics of the Cranial Base of Early Angle's Class II Division 1 Malocclusion in Permanent Teeth". In: *International Journal of Morphology* 35.2 (June 2017), pp. 589–595. ISSN: 0717-9502. DOI: 10.4067/S0717-95022017000200034. URL: http://www.scielo.cl/scielo.php?script=sci_abstract&pid=S0717-95022017000200034&lng=es&nrm=iso&tlng=en (visited on 03/08/2024).

[37] Hindol Das, Vaibhav Motghare, and Mrinalini Singh. "Human Evolution of the Teeth & Jaws: A Mouthful of History". In: (June 2021).

[38] Idit Saragusti et al. "Quantitative analysis of shape attributes based on contours and section profiles in artifact analysis". In: *Journal of Archaeological Science* 32.6 (June 2005), pp. 841–853. ISSN: 0305-4403. DOI: 10.1016/j.jas.2005.01.002. URL: https://www.sciencedirect.com/science/article/pii/S0305440305000130 (visited on 02/26/2024).

[39] Torsten Hothorn et al. "Implementing a Class of Permutation Tests: The **coin** Package". en. In: *Journal of Statistical Software* 28.8 (2008). ISSN:

1548-7660. DOI: 10.18637/jss.v028.i08. URL: http://www.jstatsoft.org/v28/i08/ (visited on 02/16/2024).

[40] H. O. Lancaster. "The Combination of Probabilities Arising from Data in Discrete Distributions". In: *Biometrika* 36.3/4 (1949). Publisher: [Oxford University Press, Biometrika Trust], pp. 370–382. ISSN: 0006-3444. DOI: 10.2307/2332674. URL: https://www.jstor.org/stable/2332674 (visited on 02/16/2024).

[41] R. D. Routledge. "Practicing Safe Statistics with the Mid-p". In: *The Canadian Journal of Statistics / La Revue Canadienne de Statistique* 22.1 (1994). Publisher: [Statistical Society of Canada, Wiley], pp. 103–110. ISSN: 0319-5724. DOI: 10.2307/3315826. URL: https://www.jstor.org/stable/3315826 (visited on 02/16/2024).

[42] Matthias Meyer et al. "Nuclear DNA sequences from the Middle Pleistocene Sima de los Huesos hominins". en. In: *Nature* 531.7595 (Mar. 2016). Publisher: Nature Publishing Group, pp. 504–507. ISSN: 1476-4687. DOI: 10.1038/nature17405. URL: https://www.nature.com/articles/nature17405 (visited on 04/18/2024).

8 supplementary figures

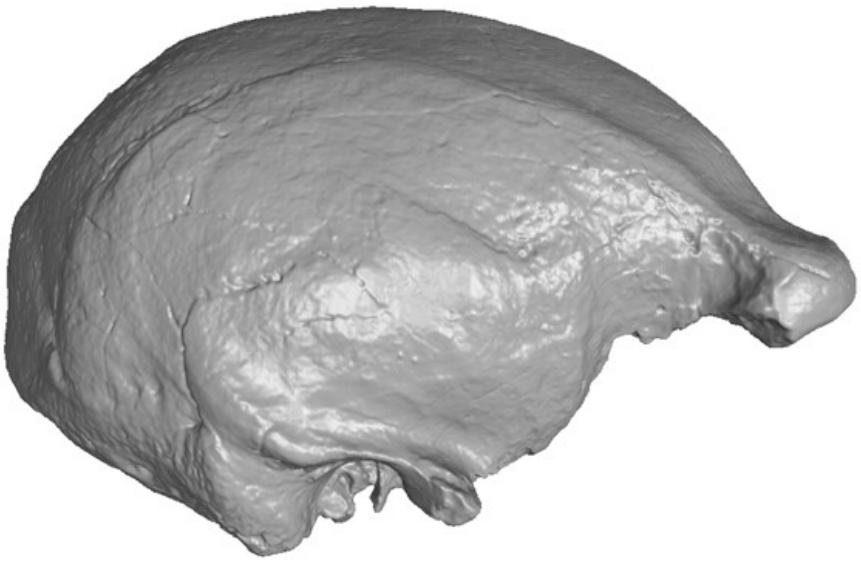

Supplementary Figure 1: Figure 1:Lateral view

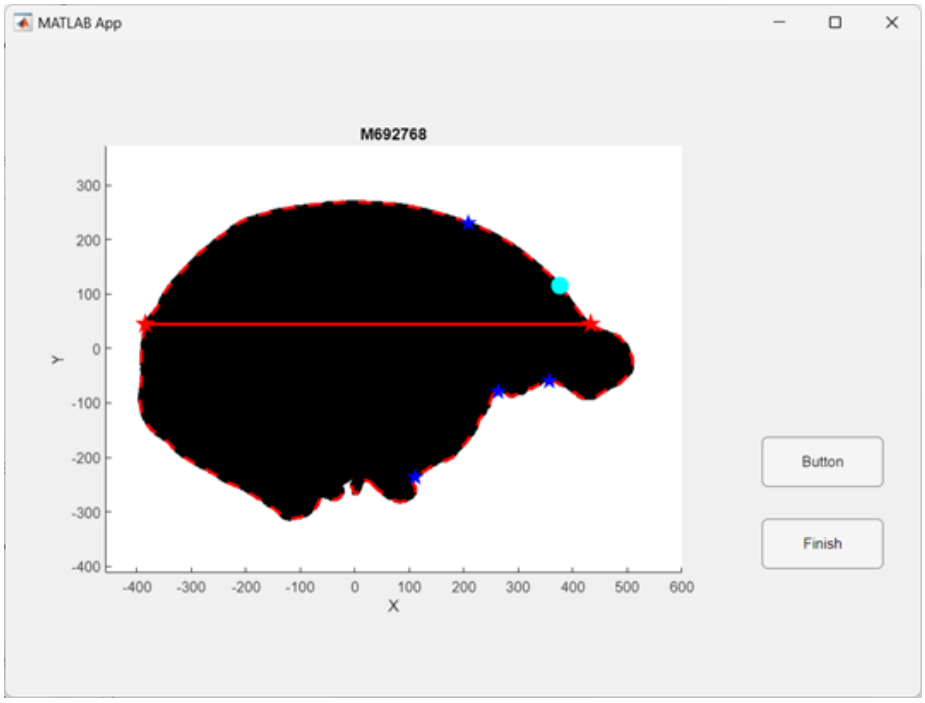

Supplementary Figure 2: Figure 1:Lateral view

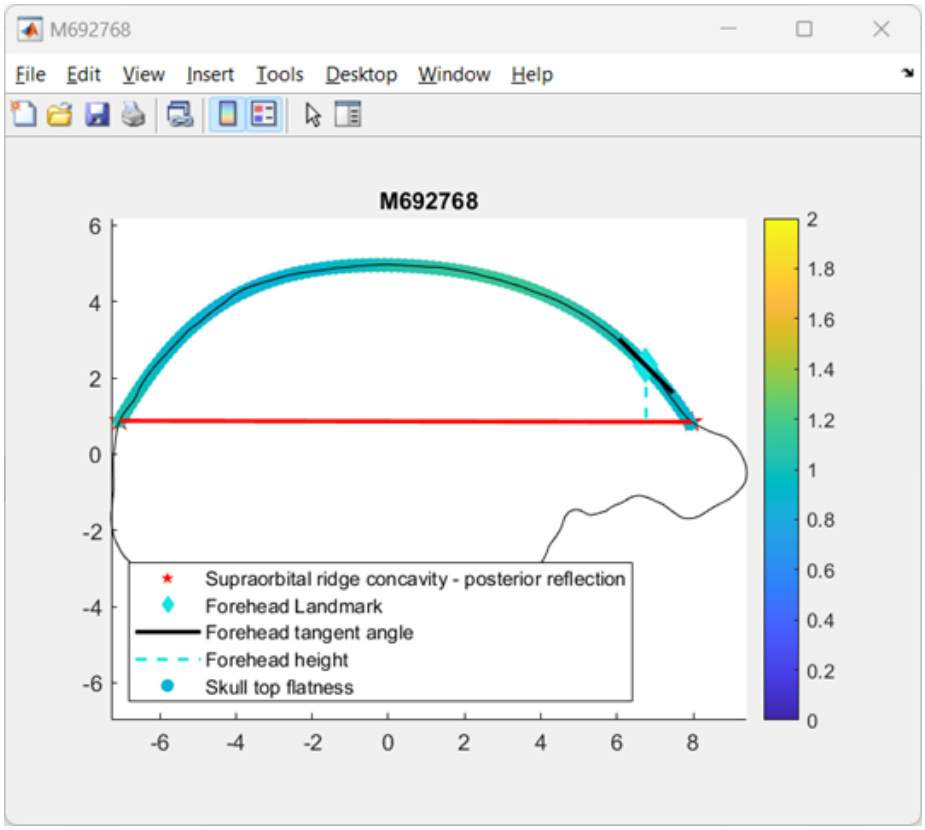

Supplementary Figure 3: Figure 1:Lateral view

Supplementary Figure 4: Figure 1:Lateral view

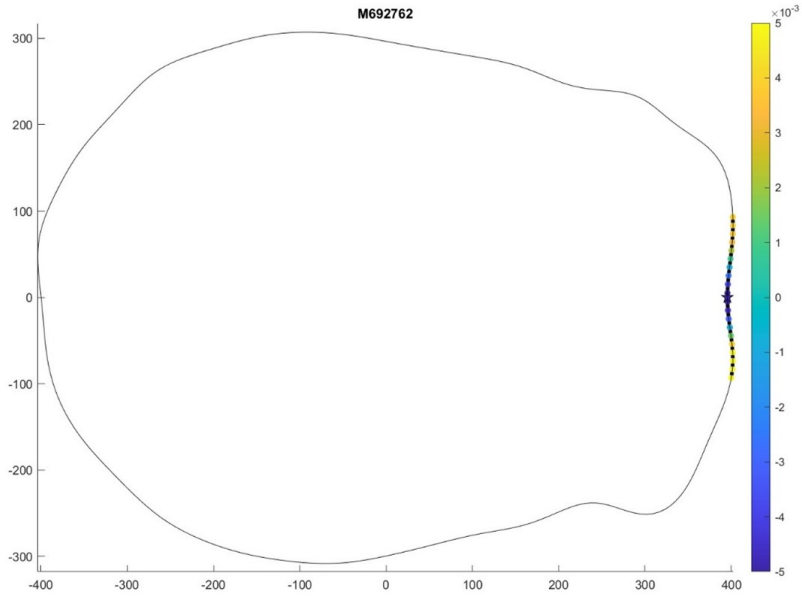

Supplementary Figure 5: Figure 1:Lateral view

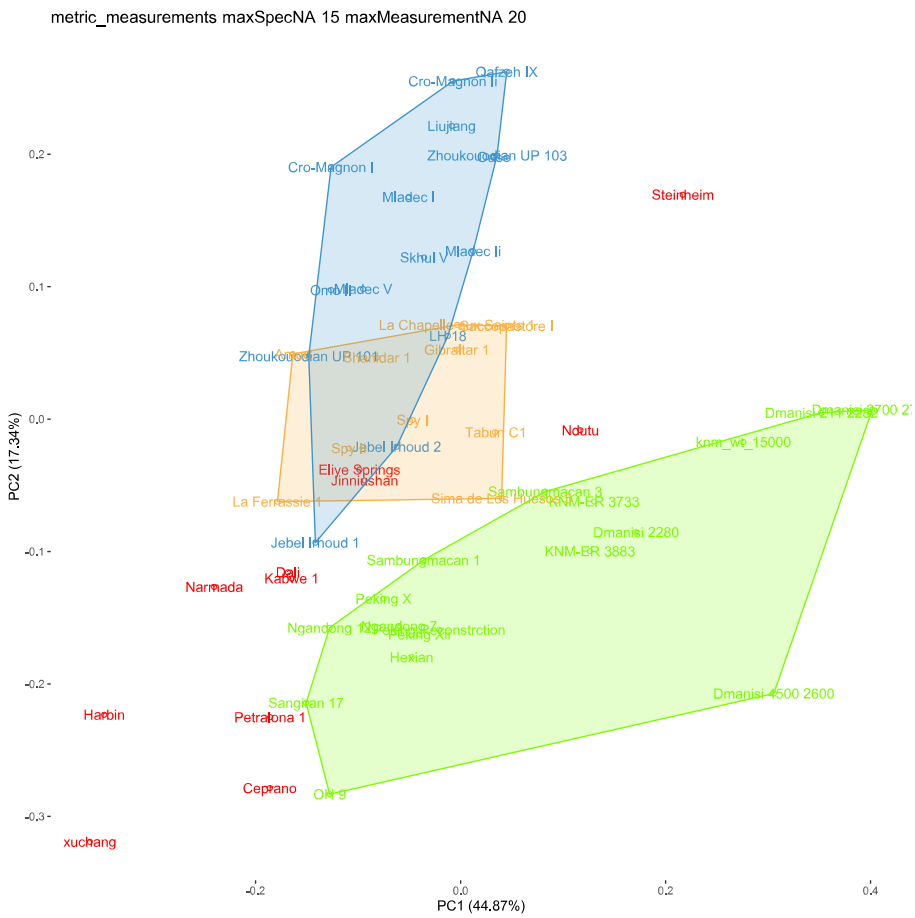

Supplementary Figure 6: metric measurements PCA

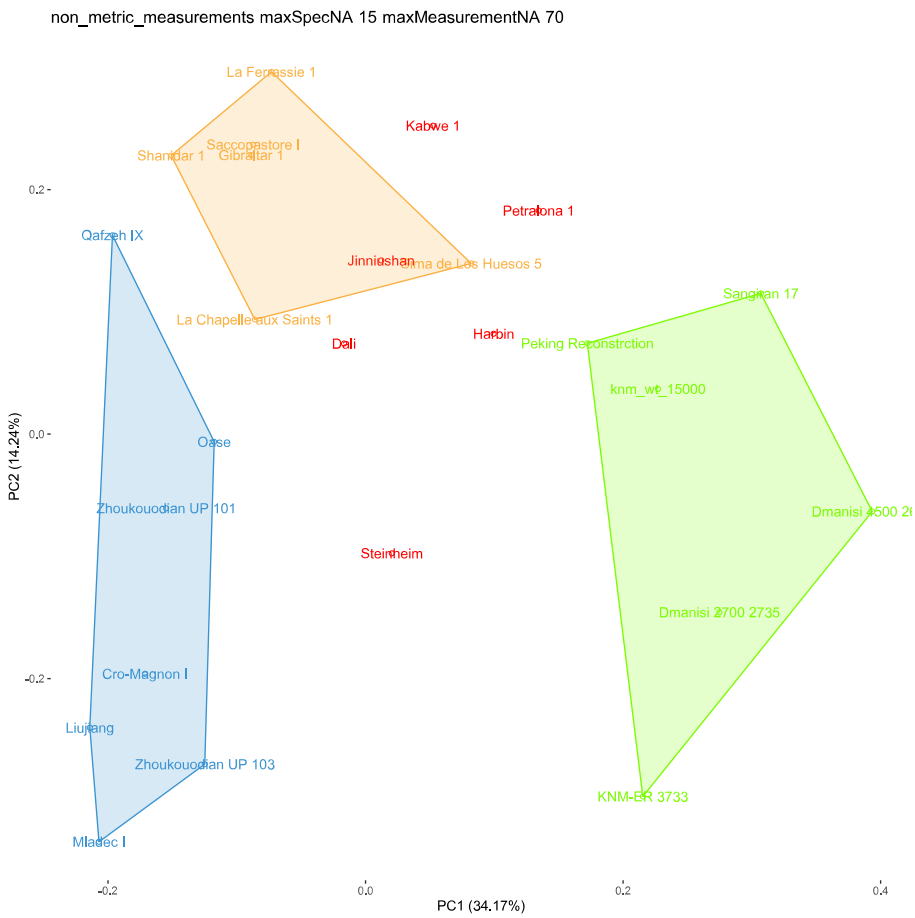

Supplementary Figure 7: non metric measurements PCA